ROLAND E. LEE, ROBERT TURNER, and RICHARD C. BENSON

OPTICAL MEASUREMENTS FOR RAMJET ENGINE DEVELOPMENT

Two optical instruments, the laser anemometer and the coherent anti-Stokes Raman scattering (CARS) spectrometer, were recently studied at APL's Propulsion Research Laboratory for use as combustion diagnostic tools. Recent test results of the laser anemometer used in a typical exhaust flow environment of a combustion chamber and of CARS in graphite surface oxidation studies are discussed.

INTRODUCTION

Advanced propulsion systems involve highly complex combustion flow processes. Extensive and accurate flowfield measurements can help to guide and support engine development. For example, in the hypersonic dual-combustor ramjet, the subsonic combustion chamber operating at fuel-rich conditions generates a complex multiphase combustion flow comprising liquid fuel droplets, soot particles, and reacting gases. The complexity of this flow is intensified by its subsequent downstream interaction with air at supersonic speeds. In such reacting flows, conventional mechanical probes can disturb the local flow environment as well as be subjected to impact and thermal damage. Optical instruments that have been developed and used in laboratory experiments of less complex combustion flows avoid these difficulties. However, their application in the harsh flow environment of ramjet engine combustion is more difficult and needs to be approached cautiously. In contrast to mechanical probes, optical instruments generally are nonintrusive; produce minimum flow disturbance; have a faster response, higher data rate capability, and better spatial resolution; and, in some cases, can measure more than one flow parameter per instrument.

Flow modeling requires accurate flowfield measurements of stream velocity, temperature and pressure distributions, and, when chemical reactions are present, the chemical species concentration distributions. For a reacting flow containing a considerable amount of particulates, the characteristics and distributions of these particles need to be measured. The particulate flow is important because it can strongly affect both the performance of optical diagnostic devices and the combustion efficiency. In relatively clean combustion flows, such as most laboratory flames, the particulates are generally of submicrometer size. In the fuel-rich ramjet flows, however, soot particles and unburned fuel droplets can extend the particle size range from submicrometer size to as large as 50 micrometers.

In principle, all of the above flow parameters may be determined by optical instruments. APL's Aeronautics Division, in collaboration with the Research Center, is currently reviewing and test-evaluating selected optical instruments for use in supersonic ramjet combustion flowfield measurements. Figure 1 lists the techniques considered and the flow parameters they are expected to measure. In some cases, an intermediate parameter is used to obtain the desired flow parameter; e.g., the laser anemometer measures particle velocity, and the gas flow velocity is deduced from modeling of particle drag.

At the onset of this program, there was very little information on the size, number density, or index of refraction of particles generated by a fuel-rich hydrocarbon combustor. The first two instruments for measuring particle size were selected on the basis of laser light transmission at two wavelengths and laser light scattering at two viewing angles. They were abandoned early in the program because analysis showed that the upper range of particle sizes of interest could not be measured. Follow-on evaluation and testing showed the laser anemometer and Raman spectrometer to be viable instruments that could withstand the hostile engine-testing environment and provide data on a number of the pertinent flow parameters. The laser anemometer observes laser light scattered by particulates embedded in the flow to deduce the particle and flow velocities, the particle size, and the particle number density. The Raman spectrometer relates the laser light scattered by molecules in the combustion medium to flow temperature and gaseous species concentrations.

The evaluation of the laser anemometer instrument included: (a) analysis with laser light scattering (Mie theory) and light diffraction computer programs; (b) calibration with a cold-air supersonic flow (Mach 3.5) with controlled particle seeding; and (c) actual measurements in a small-scale combustor that can be operated at pressures up to 4.5 atmospheres, inlet air temperatures from 650 to 870 K, and fuel-air equivalence ratios between 0.8 and 4.0, using JP-5 fuel.

PARTICLE SIZING

Various optical techniques have been developed that use scattered light to measure the micrometer-

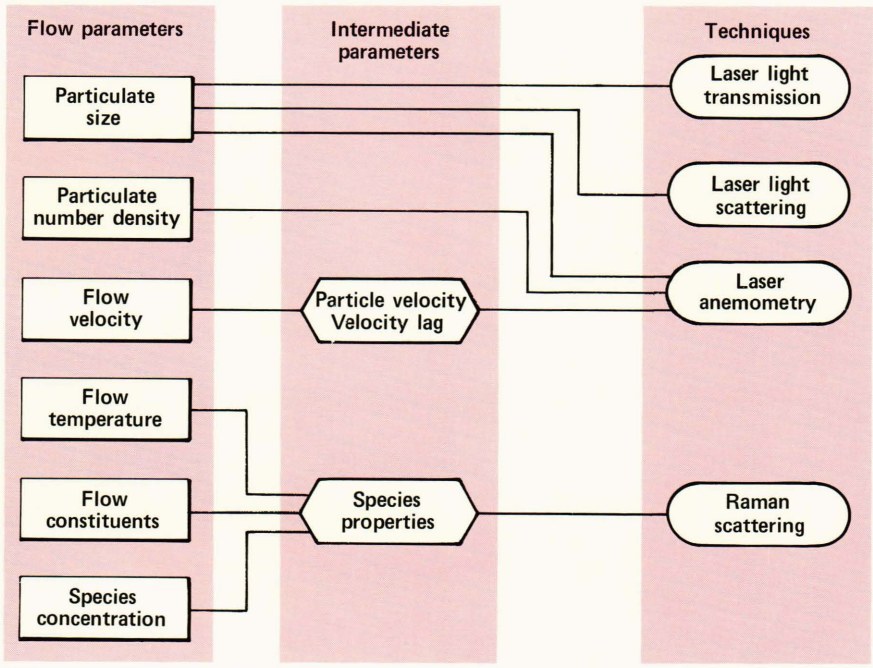

Figure 1 — Optical flow diagnostic parameters and techniques.

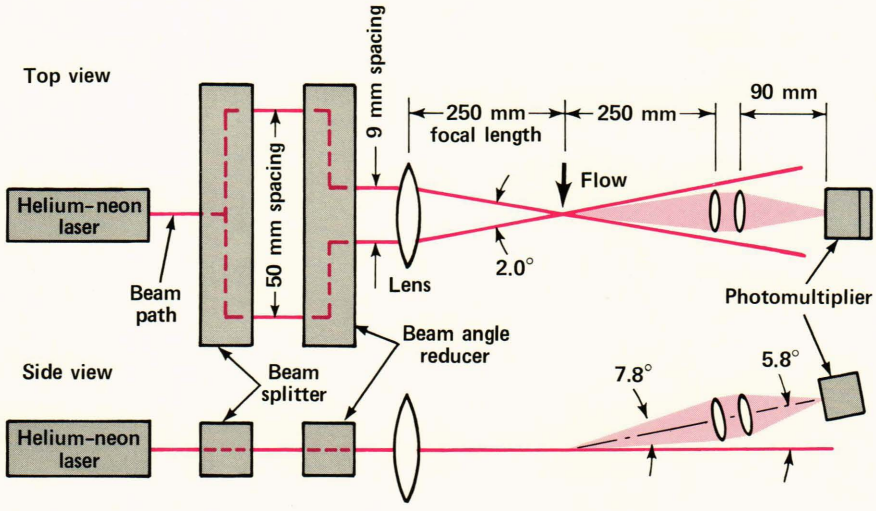

Figure 2 — Laser Doppler velocimeter optical configuration.

size particles found in combustion experiments. In general, all such techniques make assumptions about the particle size distribution, particle shape, index of refraction, and size relative to the wavelength of the light source. Some methods use relative amplitude measurements; others use absolute measurements. Some observe the signal from a single particle; others observe the signal produced by a number of particles. The actual method chosen depends to a large extent on the parameters to be determined and the adaptability of the instrument to the particular application. A standard dual-beam laser anemometer, normally used to measure particle velocity, was adapted to provide a simultaneous measurement of particle size (in the range of 3 to about 100 micrometers) and speed (550 to 1400 meters per second), the density of particles greater than about 1 micrometer, and the attenuation of a laser anemometer beam produced by particles smaller than 100 micrometers.

Figure 2 is a schematic diagram of the Thermo-Systems, Inc., laser anemometer, which uses a 5-milliwatt helium-neon laser, configured for forward scattering at an elevation angle of 5.8°. The two laser anemometer beams cross at an angle of 2° to produce an ellipsoidal scattering volume. The measured signal is a function of a particle's position in each beam; as a result, constructive and destructive interference can occur as the particle moves through the beams. It is often convenient to think of the particle as being illuminated by light and dark fringes, with a spacing of 17.6 micrometers in this case. The minor axis of the scattering volume, in the direction of flow, is 250 micrometers; the major axis, perpendicular to the flow, is 2 millimeters. A 250-micrometer aperture in the

collection optics limits the field of view at the center of the region to 16 fringes. Particles moving at speeds of 550 to 1400 meters per second will produce scattered light pulses from 0.5 to 0.2 microseconds wide that are modulated at frequencies from 30 to 80 megahertz. Figure 3 is a photograph of the laser anemometer instrument configured for use in the full-scale ramjet engine combustor.

The size of the particle producing the scattered light can be derived from the signal visibility (V), which is the ratio of the depth of the modulation of the scattered signal to the mean amplitude [$V = (I_{max} - I_{min})/(I_{max} + I_{min})$, where I_{max} and I_{min} are the maximum and minimum of the light intensities], and from the mean amplitude of the signal directly. The two methods for determining particle size are complementary. With the present laser anemometer, the intensity of the light scattered by small particles (< 3 micrometers) is low, but the visibility is high (about 1); the intensity of light scattered by large particles (> 20 micrometers) is large, but the visibility is low (less than 0.3). The intensity measurement is absolute; it generally increases monotonically with particle size and can have a large dynamic range. Visibility is a relative measurement, and because the particle size can be multivalued for a given visibility, the dynamic range is generally less than 10. This can present a problem in its application if the size range of interest is not defined beforehand. References 1 through 5 describe aspects of the visibility and scattered light measurements that are relevant to the work described here.

Particle sizing by means of the signal visibility is of recent origin, and there has been considerable discussion about its interpretation and application. The visibility and intensity techniques are both extremely sensitive to the f number of the collection optics and to their location relative to the incident laser beams. In fact, the visibility and intensity dependence on particle diameter can be tailored by the proper choice of scattering angle and collection aperture. Because of this, it is important that the instrument be calibrated and also that its response function be calculated for the conditions actually used.

Visibility curves computed for spherical particles are shown in Fig. 4 for three conditions. Curve A is calculated for the collection optics centered between the laser anemometer beams and in the plane of the beams. The visibility is approximated by:

$$V = 2[J_1(\pi D_p/\delta_f)]/(\pi D_p/\delta_f), \qquad (1)$$

where $J_1(\pi D_p/\delta_f)$ is the first-order Bessel function of $(\pi D_p/\delta_f)$, D_p is the particle diameter, and δ_f is the fringe spacing.[1] Curve B is calculated using the standard diffraction approximation for the detector mounted 5.8° above the plane of the two beams. Cal-

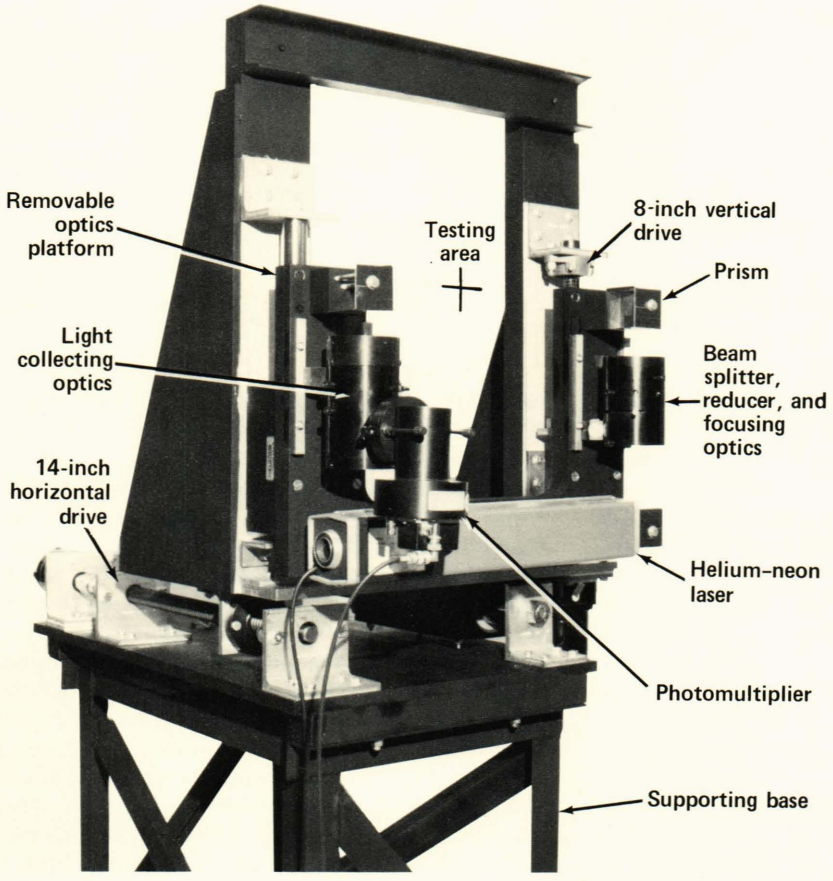

Figure 3 — Photograph of the laser Doppler velocimeter mounted on motorized two-component traverse.

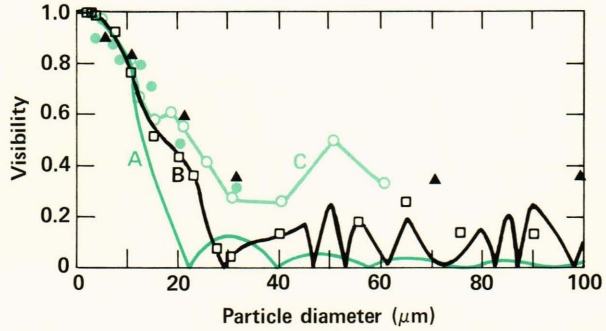

Figure 4 — Calculated and measured visibility as a function of particle diameter. The plotted data, except for A, are for a detector with a 250-millimeter focal length lens, an aperture of 34 millimeters, and a scattering angle of 5.8°. A is the visibility using the approximation of Ref. 1. B is calculated using the diffraction approximation. C, shown by the symbol ○, is the calculation using the Mie theory for dioctyl phthalate. □ indicates points calculated using Mie theory for soot-hydrocarbon particles (n = 1.67—i0.33); ▲ indicates measured values for polystyrene (n = 1.59—i0.00); and • indicates measured values for dioctyl phthalate (n = 1.49—i0.00).

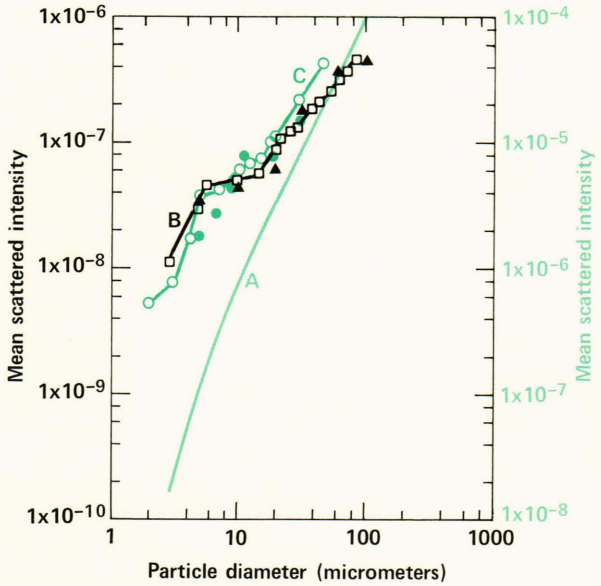

Figure 5 — Calculated and measured values of the mean scattered intensity as a function of particle size. A is the intensity calculated using the diffraction approximation with the detector centered between the beams in the plane of the laser Doppler velocimeter beams. B is the intensity calculated with the diffraction approximation at an angle of 5.8°. C, shown by the symbol ○, is the intensity calculated with the Mie theory for dioctyl phthalate. □ indicates points calculated for soot-hydrocarbon particles (n = 1.67—i0.33); ▲ indicates measured values (relative) for polystyrene (n = 1.59—i0.00); and • indicates measured values (relative) for dioctyl phthalate (n = 1.49—i0.00).

culations using the diffraction approximation are suspect when the measurements are made off-axis and the index of refraction (n) of the particle becomes a factor. In this case, the more exact Mie theory must be used.[6] The visibility calculated for selected points using the Mie theory for dioctyl phthalate (n = 1.59—i0.00) and for a soot-hydrocarbon mixture (n = 1.67—i0.33), representative of partially burned fuel, are indicated in Fig. 4. The diffraction approximation is reasonable for the expected combustion products, but the effect of the index of refraction must be considered in the calibration and for unburned fuel drops. Figure 5 shows the calculated intensities for the same two positions of the collection optics using the diffraction approximation and the Mie theory for dioctyl phthalate and the soot-hydrocarbon mixture.

The laser anemometer was calibrated with solid polystyrene spheres and liquid aerosols. Single 5- to 100-micrometer polystyrene spheres were mounted on a rotating disc that provided a particle speed of 20 meters per second. In this case, the laser anemometer output could be identified with a particle whose size, shape, index of refraction, and position in the scattering volume were known. The results of individual measurements, plotted in Figs. 4 and 5, are in reasonable agreement with the Mie theory calculations. A Bergulund-Liu aerosol generator was used to provide dioctyl phthalate aerosols up to 50 micrometers in diameter, moving at 3 meters per second (the normal velocity of the aerosols from the generator) or up to 400 meters per second when they were injected into a small supersonic wind tunnel. The results at 3 meters per second are plotted in Figs. 4 and 5. Measurements in the small wind tunnel agreed with the low-speed results for particles of up to 12 micrometers in diameter. The measurements with the larger aerosols were erratic but generally similar to those produced by smaller particles. The erratic results are attributed to the breakup of the large dioctyl phthalate drops in the high-speed flowfield.

Two selection processes are applied to each laser anemometer pulse to ensure, as far as practical, that data from only one particle are being collected and that the particle is illuminated by the maximum intensity of each incident beam. Only scattered light pulses that are less than 0.5 microseconds wide and have exactly 16 cycles of modulation are processed. Figure 6 is a simplified block diagram of the signal processing used. The laser anemometer signal is filtered with a low-pass filter to provide the mean scattered intensity $(I_{max} + I_{min})/2$; it is also filtered with a bandpass filter and rectified to give $(I_{max} - I_{min})/2$. The two outputs are stretched, sampled at their peaks, and held for 20 microseconds. The output of the bandpass filter is also used by two fast discriminators. One provides a pulse for each laser anemometer output, above a threshold equivalent to a particle larger than 1 micrometer, to start a time-to-pulse height converter and to provide a 0.5-microsecond gate and a 20-microsecond hold/reset pulse for the peak sense-and-hold circuits. The output of the second discriminator is a train of pulses equal to the number of cycles of modulation produced by the particle. If there are exactly 16 pulses, the maximum number at the center of the scattering volume, the single channel analyzer stops the time-to-pulse height

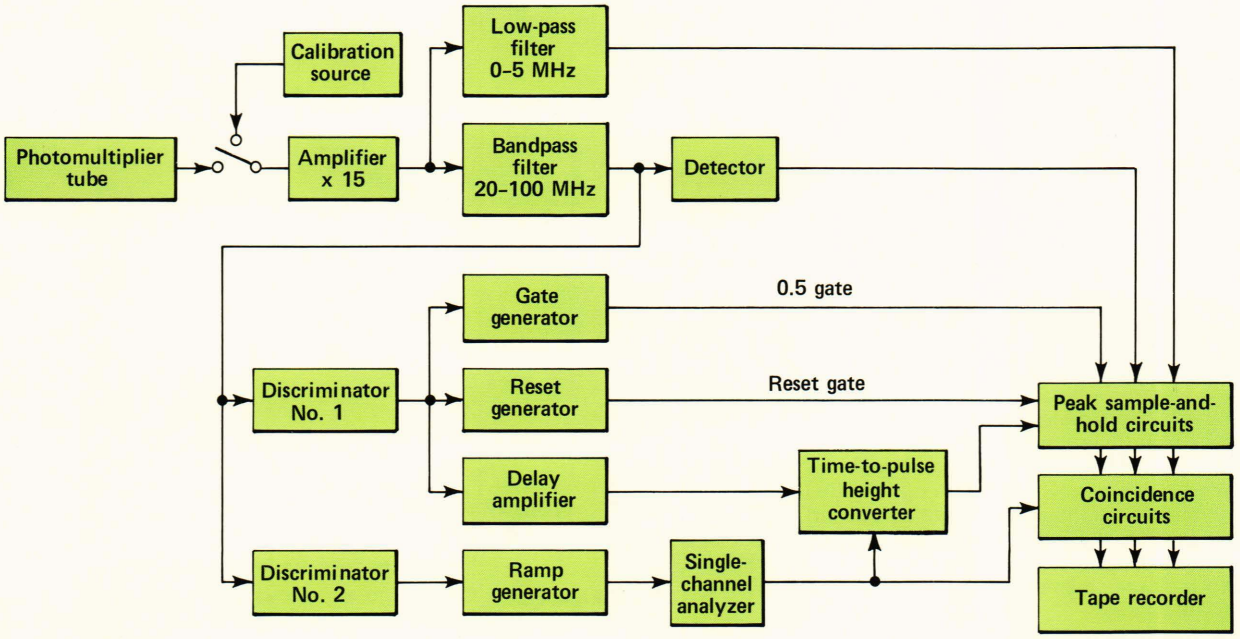

Figure 6 — Schematic of particle sizing instrument.

converter. The time-to-pulse height converter output, which is a measure of particle speed, is also sampled and held. The $(I_{max} + I_{min})/2$, $(I_{max} - I_{min})/2$, and time-to-pulse height converter voltages are recorded if a single channel analyzer pulse is present. From these data, the particle's speed and two measures of its size are derived. The output of discriminator No. 1 is also counted to indicate the flux of particles passing through the scattering volume.

The transmission ratio (I/I_0), where I is the measured intensity with the particles present and I_0 is the intensity when no particles are present, of the laser beam through the flowfield was measured to indicate the amount of material with diameters of less than about 100 micrometers in the flow, evidence of multiple scattering or refractive effects, and to reinforce the sizing results obtained from the visibility and intensity measurements. The transmission ratio is determined by the integrated effect of particle density (N), extinction efficiency (Q_{ext}), particle area (S), and path length (l) through the particulate flow:

$$I/I_0 = \exp(-\alpha l) \qquad (2)$$

where α, the attenuation coefficient per centimeter, equals $NQ_{ext}S$. The extinction efficiency is close to 2 for the large particles of interest; it is near 1 for the great number of smaller particles that contribute to the beam attenuation. Because this measurement is an average along the path of the beam through the flame, average values have been used, and an extinction efficiency of 2 has been assumed for all calculations. The path length was derived from photographs of the scattered light.

Tests were made on the fuel-rich ramjet combustor to evaluate the suitability of the instrument for the intended application and to uncover problems, resulting from refractive effects or loss of coherence, associated with the environment. Measurements were made with the laser anemometer scattering volume located on the centerline of the exhaust jet at selected distances ranging from 6.4 to 229 millimeters from the combustor nozzle exit. The combustor was operated at a nominal pressure of 240 kilopascals (35 pounds per square inch, absolute), an air inlet temperature of 650 to 870 K, and fuel-air equivalence ratios of 1.6 and 2.6 for the results described here. A typical run lasted 30 to 60 seconds, during which time particle size and velocity information was obtained on more than 1000 particles.

The spread in the measured particle diameters and speeds was large; in particular, there were large particles moving at much higher speeds than expected. Figure 7 contains plots of the average diameter, the average particle speed, and the attenuation coefficient at selected distances from the nozzle for an equivalence ratio of 1.6. In the first 50 millimeters, the speed of the particles increased from 260 to 820 meters per second; this is the region of accelerating flow. The particle speed then decreased with increasing distance to 528 meters per second, the lower limit of the instrument. The particle diameter increased in the first 50 millimeters from the nozzle, decreased for about 100 millimeters, and then increased again farther downstream.

Since small particles accelerate faster and slow down faster than large particles, and so enter or leave the velocity selection window at different times, the size distribution will be skewed to the smaller-sized particles near the nozzle and to the larger-sized particles at greater distances. This is clearly the case at distances greater than 125 centimeters from the noz-

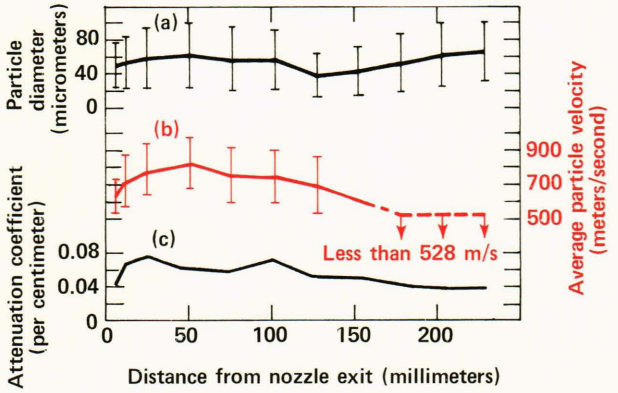

Figure 7 — The average values of the measured (a) diameter, (b) speed, and (c) attenuation coefficient, plotted as a function of distance from the exhaust nozzle for an equivalence ratio of 1.6.

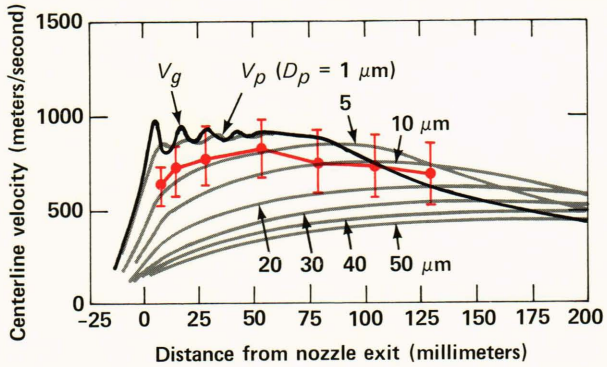

Figure 8 — Computed particle velocities for selected particle size (D_p) as a function of distance from the nozzle. The combustor pressure is 254 kilopascals, (37 pounds per square inch, absolute) and T_C = 2800°R. Velocity data for an ER of 1.6 are plotted in color.

zle. The slower particles drop below the minimum speed for which their diameter can be measured before the faster large particles do, resulting in more large particles being measured than small particles and so giving a larger average particle diameter. In general, the fluctuations of the transmitted signal increased with distance from the nozzle.

Wide variations in the particle count were observed, particularly at the greater distances; the average was about 40,000 counts per second at all positions. The number density of particles greater than about 1 micrometer was 70 particles per cubic centimeter at 12.7 millimeters from the nozzle; the value increased to 140 particles per cubic centimeter at 229 millimeters. The attenuation coefficient varied from 0.04 to 0.08 per centimeter as the distance increased from 6.4 to 229 millimeters. The large attenuation coefficient indicates that most of the particulate mass is carried by particles of less than 1 micrometer.

The results at an equivalence ratio of 2.6 were similar and consistent with those obtained at an equivalence ratio of 1.6. The maximum velocity was slightly lower (780 meters per second at 50 millimeters) and dropped off more rapidly. The attenuation coefficient was about twice that measured at the lower equivalence ratio (0.14 relative to 0.08) at the larger values, multiple scattering is becoming important. The particle count rate was approximately constant at 100,000 counts per second.

The difference between the particle velocity and the velocity of the flowfield can also be used to estimate the size of the particles in the flow. The velocity of a given size spherical particle (V_p) in a flowfield of velocity V_g was calculated using the model of Ref. 7. The model describes single particle flow in a supersonic nozzle where the particle drag coefficient is determined empirically. The gas velocity distribution was obtained as follows. For the region upstream of the nozzle exit, the one-dimensional isentropic flow equations based on the local flow cross-sectional area were used; for the near flow region downstream of the nozzle exit, V_g was obtained from a pitot probe survey of the unheated airflow. At distances of more than 90 millimeters from the nozzle, the free-circular jet approximation ($V_g \approx 1/x$) was used. The peaks in the V_g curve are related to the location of the oblique shock waves.

Figure 8 shows the computed particle speeds as a function of distance from the nozzle for spherical fuel drops 1 to 50 micrometers in diameter and for a combustor pressure of 254 kilopascals (37 pounds per square inch, absolute). In the shock region, particles larger than a few micrometers lag the gas velocity by a considerable amount. The measured velocity data for an equivalence ratio of 1.6 are also plotted on Fig. 8; they fit particles 5 micrometers or less near the nozzle and even larger particles at greater distances.

The discrepancy between the average particle size derived from the velocity lag and the laser anemometer measurements is too large to be explained by experimental error or approximations in the calculations. Since the combustor is being operated in a fuel-rich condition, most of the large particles observed are in all likelihood unburned fuel drops. The drops would be deformed into flattened, high-drag objects as they are accelerated through the nozzle and would probably break up into a large number of smaller drops, as has been observed under similar conditions, but at much lower speeds, by others. Breakup of the fuel drops can be expected when the Weber number exceeds 10 to 20. The Weber number is defined as:

$$W_e = U^2 D_p \rho_g / \sigma \qquad (3)$$

where U is the velocity of the particle relative to the flow velocity, σ is the particle surface tension, D_p is the particle diameter, and ρ_g is the gas density. At 6.4 millimeters from the nozzle, the calculated Weber number for a 50-micrometer drop of jet fuel (JP-5) is 288, far in excess of the breakup value. The large number of smaller particles after breakup scatter more energy. The actual scattered signal depends on

the number of particles in the field of view of the laser anemometer. One 50-micrometer particle is equivalent in volume to one thousand 5-micrometer particles, while only ten 5-micrometer particles are needed to give the observed signal. It is not unlikely, then, that a cluster of 10 particles, all moving at the same high speed, is in the scattering volume at one time and appears to the instrument as a single large particle.

The results of these tests indicate that the instrumented laser anemometer can be used to measure the size and speed of large solid particles in high-speed flows. However, the simultaneous measurement of size and speed indicated that particles with large measured diameters were moving faster than expected. These "large" particles are probably a number of small particles moving together in a cluster that remains after the breakup of the initial large fuel drops or the coalescence of the small drops. While the breakup of fuel drops is advantageous for their later combustion, the presence of clusters of small particles appearing to be large particles makes the interpretation of the results more difficult. The simultaneous measurement of particle size and speed is essential where particle breakup appears likely. Additional measurements with optical techniques specifically designed to measure clusters of small-size particles are required to confirm these conclusions.

COHERENT ANTI-STOKES RAMAN SCATTERING

Turning our attention from light scattered by particles to light scattered by molecules, the most common processes are illustrated in Fig. 9. Incident photons at frequency ω_0 interact with molecules and are scattered over 4π steradians with elastic and inelastic components. The elastic scattering, referred to in the past as Rayleigh scattering, is the phenomenon that results in the blue appearance of the sky and the red sun at sunrise and sunset (because shorter wavelength blue light is scattered more than red). Because the process is elastic, the scattered light is of the same frequency as the incident light; it is not specific to the molecule causing the scattering. Thus, the technique can be used for total density measurements but not for individual species concentrations.

The inelastic scattering of light by molecules is known as spontaneous Raman scattering and is termed rotational, vibrational, or electronic, depending on the nature of the energy change that occurs in the molecule. As illustrated in Fig. 9, Raman scattering consists of weak components at fixed frequency separations on both sides of ω_0. The frequency separations are related to the characteristic frequencies of the molecule, as for example, the vibrational frequency, ω_v, in Fig. 9. The Raman component that is displaced toward a longer wavelength is known as the Stokes band (ω_s) and that toward a shorter wavelength as the anti-Stokes band (ω_{as}). These bands are the result of a true scattering process; i.e., the incident photons are not absorbed and re-emitted as in

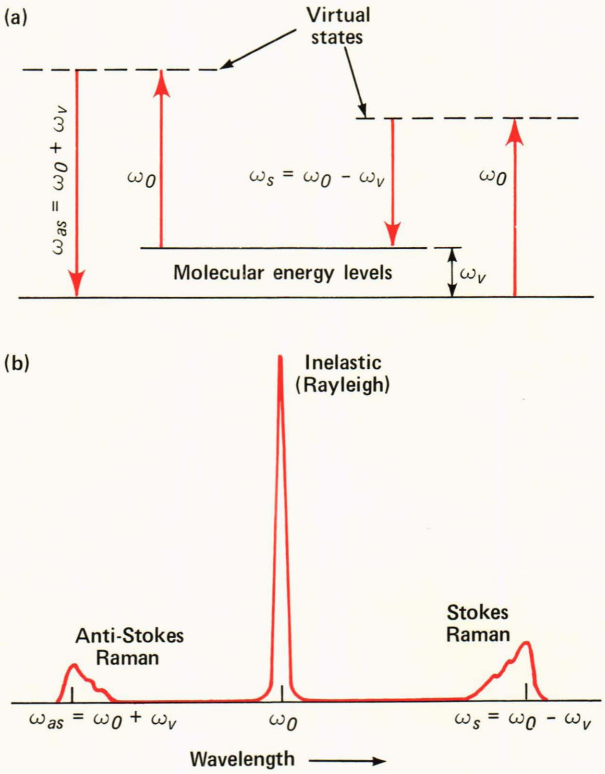

Figure 9 — Spontaneous Raman scattering. (a) Energy level diagram and (b) spectrum. The intensities are not to scale; the Raman bands are actually much weaker.

fluorescence. Hence, any incident wavelength can be used, although visible radiation is preferred because of the high sensitivity of detectors in the visible region and the fact that the intensity of the Raman scattering scales as ω_0^4. In vibrational Raman scattering, the interaction between the radiation and the sample depends on the vibrational modes of the molecule and is, therefore, species specific. Because the energy distribution in the vibrational modes depends on the molecular temperature, the spectral distribution of the Raman scattering can be used to measure the gas temperature, which is assumed to be equal to the molecular temperature. In addition to the ω_0^4 dependence, the Raman scattering intensity is linearly proportional to the species number density and the power of the incident laser.

Unfortunately, spontaneous Raman scattering is a very weak effect and usually is not amenable to practical combustion diagnostics. However, the advent of high-power lasers made it possible to devise new Raman processes that result in larger signals. One such process is coherent anti-Stokes Raman scattering (CARS). Although CARS was discovered in the early '60s,[8] it was not until the mid-seventies when high-peak-power tunable lasers became generally available that investigations of the technique became widespread. Numerous experiments in CARS have been conducted on laboratory flames,[9-11] and intensive work is in progress at various development labo-

ratories to use it as a nonintrusive probe of jet engines.

In CARS two laser beams at the frequencies ω_1 and ω_2 interact with the sample molecules in a nonlinear manner to generate a new coherent beam at frequency $\omega_3 = 2\omega_1 - \omega_2$, as illustrated in Fig. 10. When the frequency difference $\omega_1 - \omega_2$ is close to the vibrational frequency, ω_v, of a Raman active mode, the magnitude of the CARS signal at ω_3 becomes very large. The incident beams, however, must be aligned so that the nonlinear interaction is properly phased. In gases, phase matching can occur when the beams are collinear. Although this is easy to produce optically, the interaction length is rather long, leading to poor spatial resolution. The problem is overcome by separating the incident beams and crossing them at the correct phase-matching angles.

A narrowband laser at a fixed frequency is used to generate ω_1, and, since $\omega_1 - \omega_2$ must be varied to coincide with a molecular resonance, ω_2 must be obtained from a tunable source such as a dye laser. There are two methods of tuning ω_2 to generate the CARS spectrum. In one, ω_2 is generated from a narrowband dye laser, and the CARS spectrum is obtained by scanning the dye laser frequency and using a single channel detector. In the other method, ω_2 is generated from a broadband dye laser and the entire CARS spectrum can be obtained simultaneously for several species using a multichannel detector. Although the latter approach is not as sensitive, it allows fast time-resolved measurements to be made on fluctuating phenomena.

The CARS instrument being tested at APL is modeled after that developed by Eckbreth at the United Technologies Research Center.[10,12] A schematic of the optical configuration is shown in Fig. 11. A frequency-doubled Nd:YAG laser is used to generate the primary beam (ω_1) at a wavelength of 532 nanometers. Because frequency doublers are not 100% efficient, there is residual 1064-nanometer radiation from the laser that can be utilized by passing it through a second frequency doubler (KD*P crystal). This additional 532-nanometer beam pumps a dye laser that produces a broadband output centered at ω_2. The dye laser beam and the pump beam are adjusted to the same diameter using Galilean telescopes, ensuring optimum focusing of the beams. (The prisms and half-wave plates are used in polarization-dependent experiments.) The pump beam is split into two components that can be directed independently to the focusing lens; a rotatable optical flat allows for minor steering of the dye laser beam. This

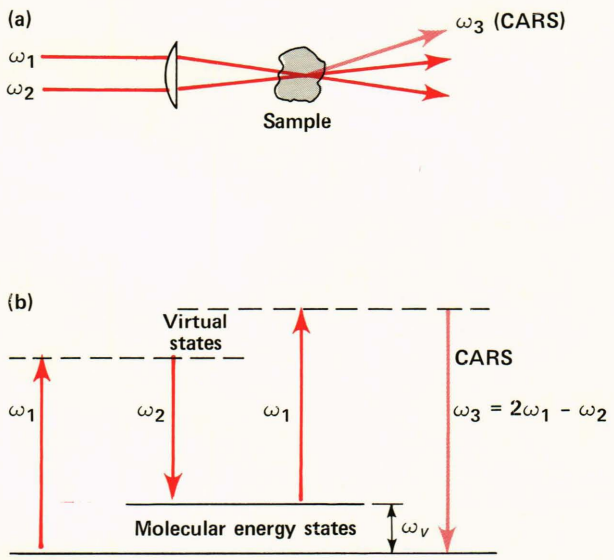

Figure 10 — Coherent anti-Stokes Raman scattering. (a) General approach and (b) energy level diagram.

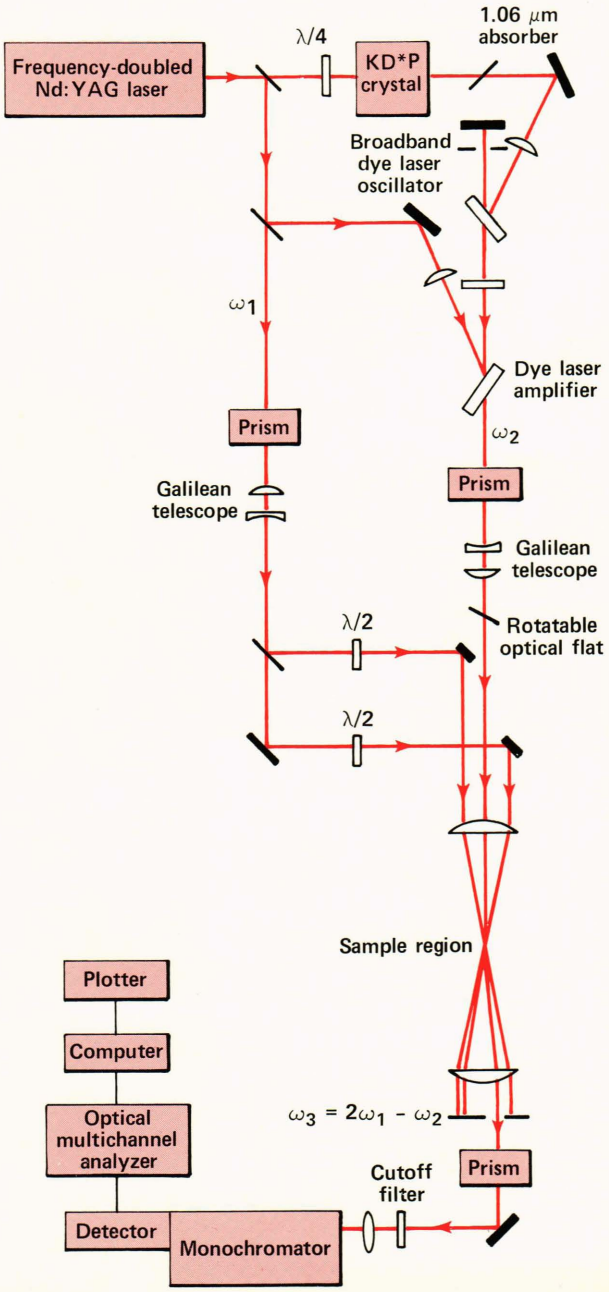

Figure 11 — Schematic of CARS system.

enables the beams to be aligned at the proper angles for phase matching, while achieving good spatial resolution in the focal region. After being focused into the medium, the incident beams and the newly generated CARS beam are recollimated by a collection lens. The CARS beam, which is spatially separated from the other beams, passes through an aperture and a cutoff filter and is then detected by an optical multichannel analyzer.

From a systems standpoint, spontaneous Raman scattering has several advantages over the CARS technique, the most important being that it is much simpler in both optical layout and interpretation of data. The relationship between the Raman signal and the species concentration and temperature is straightforward. The spatial resolution, approximately 20 micrometers for lenses of moderate focal length, is excellent. Unfortunately, those advantages are often outweighed by low sensitivity and, especially in combustion applications, by background luminosity and laser-induced interferences such as fluorescence and particulate incandescence. The CARS technique, although much more complex than the spontaneous Raman method, overcomes most of the disadvantages of the latter when probing combustion processes. CARS is a rather strong process that results in signal levels many orders of magnitude larger than those from spontaneous Raman scattering. Because the CARS radiation is itself essentially a laser beam, all of it can be collected. On the other hand, in spontaneous Raman scattering the photons are scattered over 4π steradians and are collected only over a limited solid angle. A more important consequence of the coherent nature of the CARS radiation is that it can be spatially separated (normally with just an aperture) from the incident pump beams, and elaborate double monochromators are not required. Because only a very small solid angle is required to collect all of the CARS radiation, interferences from background luminosity and laser-induced particulate incandescence are small. Furthermore, the CARS beam is in a spectral region (the anti-Stokes region) that is free of laser-induced fluorescence.

Despite all of the significant advantages of CARS, there are a few disadvantages. Although the signal is rather intense, the sensitivity is limited by interferences from the nonresonant background. Polarization-dependent experiments have recently been used to suppress this background but at a cost of losing some of the desired CARS signal. The spatial resolution is not as good as in spontaneous Raman scattering, with typical interaction regions 1 millimeter long and 0.2 millimeter in diameter. Another disadvantage is the complex dependence of the CARS signal on species concentration and temperature; that dependence requires extensive analysis and calibration.

The initial work on CARS at APL has used the technique to measure the concentration of gaseous species near a hot graphite surface in various oxidizing environments. The experimental results will be used to improve the theoretical procedure for predicting the amount of material loss resulting from ablation in supersonic ramjet combustors. Preliminary measurements using the existing ablation apparatus were encouraging in that carbon monoxide produced during the oxidation of graphite was detected with moderate spatial resolution. It should be noted that spontaneous Raman scattering could not be used in this application because of the extremely bright incandescence from the hot graphite surface. However, the entire CARS signal can be collected using small solid-angle optics, which eliminated most of the incandescent background. Improvements to the ablation apparatus and the CARS system are in progress so that accurate measurements of species concentration can be made as a function of distance above the ablating surface.

CONCLUSIONS

Because of their nonintrusive nature, fast time response, and high spatial resolution, optical measuring devices are attractive for measuring complex and unstable combustion flowfields. Because of their limitations, however, their application must be scrutinized carefully, and they must be well calibrated and adapted to the environment. The importance of these points was clearly demonstrated in the application of a laser anemometer for particle sizing.

REFERENCES

1. W. M. Farmer, "Measurement of Particle Size, Number Density and Velocity Using a Laser Interferometer," *Appl. Opt.* **11**, 2603 (1972).
2. W. M. Farmer, "Observations of Large Particles with a Laser Interferometer," *Appl. Opt.* **13**, 610 (1974).
3. W. M. Farmer, "Visibility of Large Spheres Observed with a Laser Velocimeter: A Simple Model," *Appl. Opt.* **19**, 3660 (1980).
4. D. Holve and S. A. Self, "Optical Particle Sizing for in Situ Measurements," Parts 1 and 2, *Appl. Opt.* **18**, 1632 (1979).
5. F. Durst, "Review-Combined Measurements of Particle Velocities, Size Distributions, and Concentrations," *J. Fluids Eng.* **104**, 284 (1982).
6. G. Grehan and G. Gouesbet, "Mie Theory Calculations – New Progress, with Emphasis on Particle Sizing," *Appl. Opt.* **18**, 3489 (1979).
7. W. J. Yanta, "Measurements of Aerosol Size Distribution with a Laser Doppler Velocimeter (LDV)," in *Aerosol Measurements,* NBS special publication 412, pp. 73-88 (7 May 1974).
8. P. D. Maker and R. W. Terhune, "Study of Optical Effects due to an Induced Polarization Third Order in Electric Field Strength," *Phys. Rev.* **137A**, 801 (1965).
9. W. M. Tolles, J. W. Nibler, J. R. McDonald, and A. B. Harvey, "A Review of the Theory and Application of Coherent Anti-Stokes Raman Spectroscopy (CARS)," *Appl. Spectrosc.* **31**, 253 (1977).
10. A. C. Eckbreth, P. A. Bonczyk, and J. F. Verdieck, "Combustion Diagnostics by Laser Raman and Fluorescence Techniques," *Prog. Energy Combust. Sci.* **5**, 253 (1979).
11. G. L. Eesley, *Coherent Raman Spectroscopy,* Pergamon Press, New York (1981).
12. A. C. Eckbreth, "BOXCARS: Cross-Beam Phase-Matched CARS Generation in Gases," *Appl. Phys. Lett.* **32**, 421 (1978).

ACKNOWLEDGMENTS – We would like to acknowledge the assistance of the following people in the various aspects of this work: R. A. Murphy and S. Favin of the Research Center in the particle sizing experiment; J. Funk and C. E. Stevens of the Propulsion Research Laboratory in the actual combustor measurements in the test cell; and H. Y. Chiu in the CARS experiments on graphite ablation. We would also like to thank A. C. Eckbreth of the United Technology Research Center for help in the design of the CARS system and R. Antcliff and O. Jarrett of NASA Langley for help in the initial checkout of CARS.